CRACK KINKING IN LASER WELDS - EXPERIMENTS AND MODELLING

W. BROCKS, P. NÈGRE & D. STEGLICH

Institute for Material Research, GKSS Research Centre, D-21502 Geesthacht, Germany

ABSTRACT

Ductile tearing of undermatched laser-welded high-strength aluminium sheets is studied both experimentally and numerically. The mechanical behaviour of the various material zones, base metal, heat affected zones and fusion zone, was characterised by means of micro-flat tensile specimens, and the respective microstructures were quantitatively analysed. Fracture tests have been carried out on compact specimens with initial cracks being positioned in the base metal, in the fusion zone and in the heat affected zone close to the fusion zone. The latter often deviate into the softer weld material.

All the three crack configurations have been numerically simulated by two models, namely the micro-mechanically based damage model of Gurson, Tvergaard and Needleman (GTN) and a cohesive model (CM) based on a phenomenological traction-separation law. The present contribution focusses on the third crack configuration, i.e. an initial crack close to the interface between FZ and HAZ, where crack kinking into the softer FZ has been observed in the experiments. The stress-strain curves of the various materials are determined from the test data of the micro-flat tensile specimens. The initial void volume fraction used in the GTN model is obtained from microstructural observations. The parameters of the CM, cohesive strength and separation energy, are determined phenomenologically by comparing the results of numerical simulations with experimental data from fracture tests with cracks propagating in the respective homogeneous materials, base and weld metal.

The parameters are then applied to the case of cracks at the interface between fusion zone and heat affected zone. Crack kinking could indeed be predicted with both models. Comparisons based on load vs CMOD curves as well as CTOD resistance curves generally show a satisfactory agreement between experimental results and numerical simulations.

1 INTRODUCTION

New aluminium alloys have been developed to satisfy the demands of transportation industries for high strength, improved damage resistance as well as reduced production cost. Al-Mg-Si alloys of the 6xxx series are considered as an eventual replacement for Al 2024 in aircraft industries [1]. They have medium to high strength, good corrosion properties and an improved fracture toughness [2], and they can be joined by modern welding technologies such as laser-beam welding (LBW). The high energy density introduced into the workpiece during laser welding allows the formation of narrow, fully penetrating welds. The reduced size of the weld limits the problems like microstructural changes, porosity formation due to gas entrapment, crack sensitivity and loss of strength in the weld and heat affected zone.

A weld is characterised by three main zones: the weld or fusion zone (FZ), the heat affected zone (HAZ) and the base material (BM), which is not affected by the welding process. The FZ has a lower strength than the BM and the HAZ in the case of aluminium welds, which is called "undermatching" with a mismatch ratio of $\sigma_y^{FZ}/\sigma_y^{BM} < 1$. Due to the heat input during welding and possible use of filler material, the microstructures in the different zones vary. Two populations of large particles and dispersoids are found in Al 6xxx alloys. The large particles consist either of an intermetallic phase Mg_2Si, which is responsible for the high strength, or of an Fe-rich phase. The dispersoids contain Al-Mn-Si. The coarse particles can either fracture or debond from the matrix, depending on their size and morphology. Therefore, they are regarded as nucleation sites

for damage. Particle size and morphology vary between the various zones of the welded joint.
Numerical simulations of crack extension under monotonic loading were performed for Al 6xxx sheet metal [3] as well as for aluminium welds [4]. Laser beam welds of an Al 6xxx alloy were investigated in a European project. The fracture behaviour was studied by testing and numerical simulations for three positions of the initial crack, namely within the BM, in the centre of the FZ, and in the HAZ close to the interface to the FZ. All the three crack configurations have been numerically simulated by two models, namely the micro-mechanically based damage model of Gurson, Tvergaard and Needleman (GTN) and a cohesive model (CM) based on a phenomenological traction-separation law.
The mechanical behaviour of the three material zones has been characterised by tests on micro-flat tensile specimens, and the respective microstructures have been analysed by quantitative metallography. The yield strength of BM and FZ is 302 MPa and 203 MPa, respectively, which results in a mismatch ratio of 0.67. The volume fraction of particles in the FZ is 3.5%, which is taken as initial void volume fraction in the GTN model.
The present contribution focusses on the third crack configuration, i.e. an initial crack in the HAZ close to the interface between FZ and HAZ, where crack kinking into the softer FZ has been observed, see Figure 1.

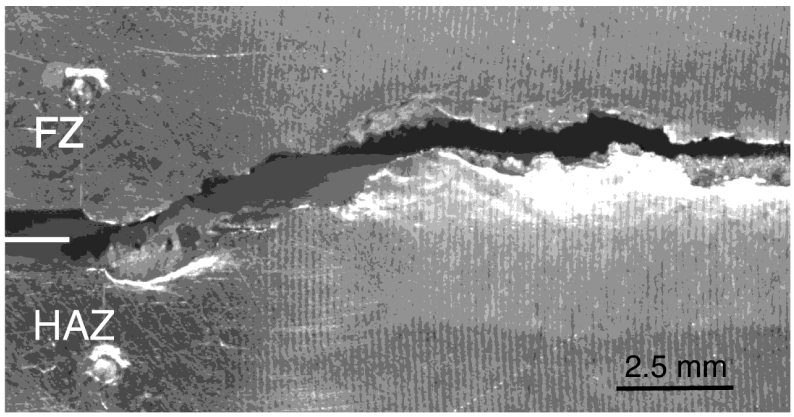

Figure 1: Kinking of a HAZ crack into the FZ.

2 MODELLING APPROACH

Models of porous metal plasticity are used to describe the micromechanical mechanisms of void nucleation, growth and coalescence in the framework of continuum mechanics. The damage parameters are related to microstructural properties of the respective material. The yield condition for a porous plastic solid was first derived by Gurson [5] and later modified by Tvergaard and Needleman [6],

$$\Phi = \left(\frac{\Sigma_e}{\sigma(\varepsilon^p)} \right)^2 + 2 f^* q_1 \cosh\left(\frac{3 q_2 \Sigma_h}{2 \sigma(\varepsilon^p)} \right) - 1 - \left(q_1 f^* \right)^2 = 0 \ . \qquad (1)$$

Damage is described by the internal variable f^*, which is a function of the void volume fraction, f. The rate of f is proportional to the plastic volume dilatation rate, if no void nucleation is considered. Three parameters describe the evolution of void growth from initial porosity, f_0, up to coalescence, f_c, and final failure, f_f. The initial void volume fractions, f_0, for BM and FZ have been determined by quantitative metallography. An additional length-scale parameter appears in form of the mesh size in the crack ligament. The physical representation of the required internal lengthscale for damage models is the average spacing of inclusions in a material. The correlation of material and model length scales is established by assuming equivalence of dissipated energy [7, 8]. For further details of the mechanical characterisation and parameter identification for BM and FZ see [9].

The idea of the *cohesive model* goes back to considerations by Barenblatt. In modern applications, interface elements transferring cohesive stresses, $\boldsymbol{\sigma}$, which generally have one normal (mode I) and two tangential (mode II, III) components, are introduced between the continuum elements, which obey a separation law, $\boldsymbol{\sigma} = \boldsymbol{f}(\boldsymbol{\delta})$, where $\boldsymbol{\delta} = [\mathbf{u}]$ is the vector of the displacement jump between adjacent continuum elements. This cohesive law is purely phenomenological, and no possibilities exist for measuring it directly. It has obviously to be chosen in dependence on the micromechanical damage mechanism leading to fracture. In the present simulations, the following cohesive law was applied [10],

$$\sigma = \sigma_c \begin{cases} 2\left(\frac{\delta}{\delta_1}\right) - \left(\frac{\delta}{\delta_1}\right)^3 & \text{for } \delta \le \delta_1 \\ 1 & \text{for } \delta_2 \le \delta \le \delta_c \\ 2\left(\frac{\delta - \delta_2}{\delta_c - \delta_2}\right)^3 - 3\left(\frac{\delta - \delta_2}{\delta_c - \delta_2}\right)^2 & \text{for } \delta_2 \le \delta \le \delta_c \end{cases}, \qquad (2)$$

with $\delta_1 = 0.01\ \delta_0$, $\delta_2 = 0.05\ \delta_0$ and two material parameters, cohesive strength, σ_c. and critical separation, δ_c. Instead of δ_c. the work of separation, $\Gamma_c \approx 0.51 \sigma_c \delta_c$, represented by the area under the stress vs. separation curve, may be taken as material parameter. As the internal length scale is introduced via δ_c, the mesh size has no physical significance. A general procedure for the determination of the parameters, σ_c and Γ_c, for normal fracture, has been proposed in [11]. In the present study, they have been determined phenomenologically by comparing the results of numerical simulations with experimental data from fracture tests with cracks propagating in the homogeneous materials, BM and FZ, respectively. The cohesive law (2) can be generalised for other fracture modes with three independent parameter sets in total. In mixed-mode situations like crack kinking, however, the respective separation processes will interact, and the cohesive law has to account for this interaction [10].

As the material properties of the HAZ vary quite strongly and as the exact location of initial cracks in the tests was not reproducible, the numerical simulations restrict to a bimaterial configuration with the initial crack located exactly at the interface. The mechanical properties of the HAZ material close to the FZ accord with those of the BM.

Whereas the FE mesh for the CM is 2D, plane stress, the GTN model requires a 3D mesh due to the low stress triaxiality in plane stress situations which would inhibit void growth.

3 RESULTS

The tests were performed on C(T) specimens of width $W = 50$ mm, thickness $B = 4.2$ mm, $a_0/W = 0.5$. The FZ is 2.8 mm wide, and the HAZ 9 mm. Force, crack mouth opening (CMOD) and crack tip opening displacement (CTOD) were recorded during the tests. The CTOD, δ_5, is measured between two indentation points at the specimen surface being 5 mm apart and located at the initial crack tip [12]. It is particularly suited to characterise ductile tearing resistance in thin, inhomogenoeus specimens. Crack extension, Δa, was measured after termination of the test. The CTOD R-curves were thus obtained by a multiple specimen technique. The load vs CMOD curves respresent single tests. Crack path deviation was observed for some initial cracks located close to the interface between FZ and HAZ, see Figure 1. No respective R-curve can be presented, however, due to the multiple specimen technique, as the exact location of initial cracks in the tests was not reproducible. The numerical simulations of an interface crack are hence compared to the experimental results for cracks extending in the FZ and the HAZ, which are supposed to give lower and upper bounds.

Figure 2 shows the results of the numerical simulations with the GTN model. The initial void volume fraction for the FZ is $f_c = 0{,}035$. The void volume fraction at coalescence has been varied between $f_c = 0{,}065$ and $f_c = 0{,}075$. The element size is $70 \times 150 \times 210\ \mu m^3$. Maximum load is satisfactorily met by the simulations, but the load drop beyond maximum load is too slow, see Figure 2a. A comparison with purely elasto-plastic constitutive behaviour, i.e. not accounting for damage and crack extension, see curve "von Mises", reveals that the crack initiates far below

maximum load. Any assessment based on crack initiation would hence significantly underestimate the real residual strength The predicted R-curves lie within the scatter of the experimental values, Figure 2b. Note, that f_f does not affect the initiation value of CTOD but only the slope of the R-curve.

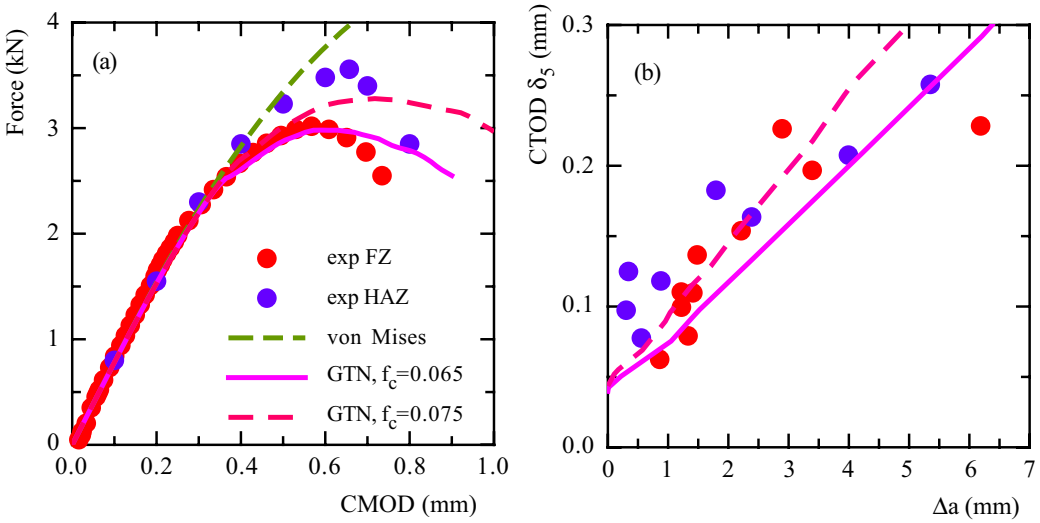

Figure 2: Load vs CMOD (a) and δ_{5R}-curve (b) of laser-welded C(T) specimens, experiments with FZ and HAZ cracks and numerical simulations of interface crack with GTN model

Figure 3 displays the variation of the damage variable, f, at the crack tip. Red colour denotes completely damaged elements, $f = f_f = 0.15$. Starting from the interface between FZ and HAZ (BM properties) , the crack deviates into the FZ as was observed experimentally, see Figure 1.

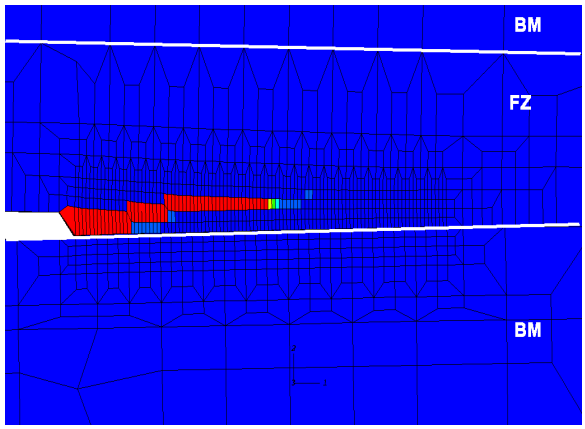

Figure 3: FE simulation of interface crack with GTN model, f_c = 0,075, kinking into FZ.

The respective results of the numerical simulations with the cohesive model are shown in Figure 4. The cohesive strengths for mode I and mode II $\sigma_{Ic} = 500$ MPa and $\sigma_{IIc} = 200$ MPa, respectively, and the separation energies $\Gamma_{Ic} = \Gamma_{IIc} = 15$ kJm^{-2}. Note that $\delta_{Ic} = 0.059$ mm is approximately equal to the CTOD at initiation, see Figure 2b. Maximum load and the load drop beyond maximum load are well met, Figure 4a. The predicted R-curve lies within the scatter of the experimental values, Figure 4b.

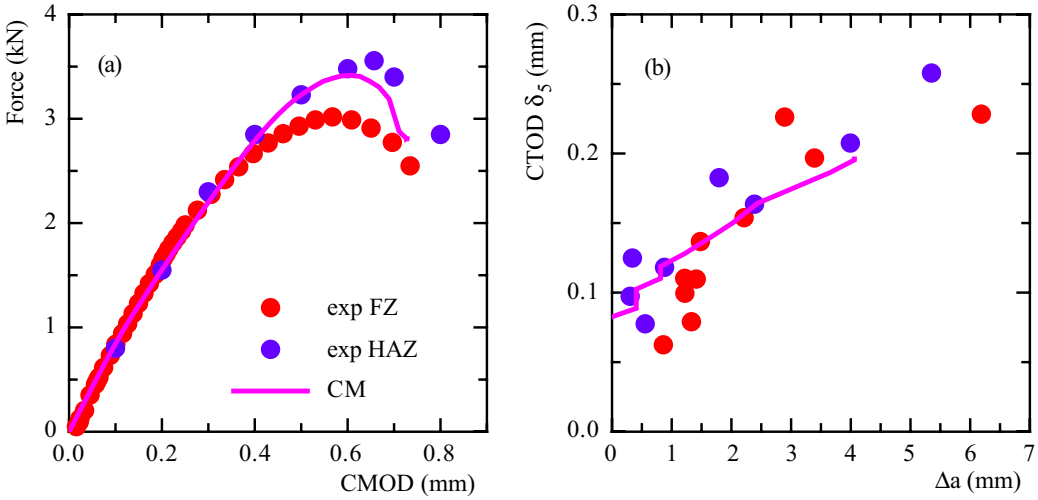

Figure 4: Load vs CMOD (a) and δ_{5R}-curve (b) of laser-welded C(T) specimens, experiments with FZ and HAZ cracks and numerical simulation of interface crack with cohesive model

The deformed mesh at the crack tip is displayed in Figure 5. Crack extension occurs as separation between continuum elements. Again, the crack deviates into the FZ starting from the interface between FZ and HAZ (BM properties).

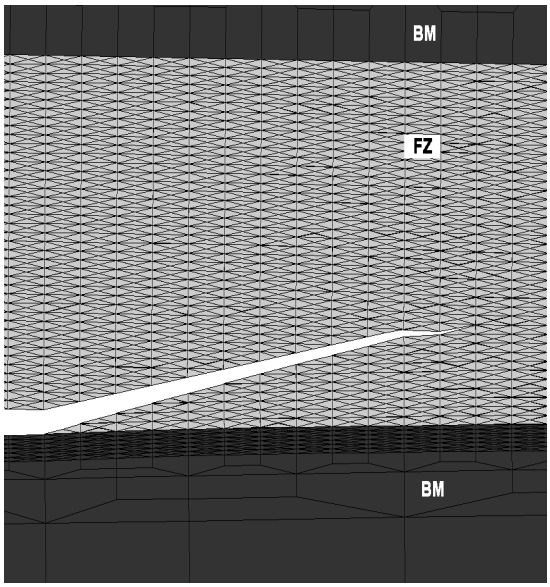

Figure 5: FE simulation of interface crack with cohesive model: kinking into FZ.

4 CONCLUSIONS

Crack extension along a bimaterial interface, namely the HAZ and the FZ of a laser welded Al panel has been studied. This case is of high practical interest, as cracks in welded components may deviate into zones of lowest strength, i.e. the BM for overmatched and the FZ for undermatched welds. Any deviation of the crack path from an orientation normal to the external loading significantly affects the macroscopically measured fracture toughness. As the material properties of the HAZ vary quite strongly and as the exact location of initial cracks in the tests was not reproducible, the numerical model assumes an interface crack in a bimaterial system (FZ / BM).

The GTN model requires a 3D mesh due to the low stress triaxiality in plane stress situations. The parameters were taken from the simulations of pure FZ cracks. The FE mesh for the CM is 2D, plane stress. The cohesive law has to account for mode II separation, if the crack does not extend perpendicular to the loading direction. Crack path deviation could be simulated with both models but was found to be strongly affected by the mesh design and the model parameters, particularly f_c and q_2 for the GTN model and the mode interaction within the cohesive law.

The investigations demonstrate that crack extension can be simulated by both models even for quite sophisticated problems like welded joints. Identifying the material properties for the various material zones is a challenging task, however, requiring experience and non-standard experimental methods. Any prediction of an R-curve for a crack in a graded material may suffer from inherent uncertainties of the test conditions, namely the precise location of the crack and the local mechanical properties.

5 REFERENCES

[1] Ehrström, J., Warner, T.: Metallurgical design of alloys for aerospace structures, Material Science Forum 331-337 (2000), 5-16.

[2] Urreta, S.E., Louchet, F., and Ghilarducci, A.: Fracture behaviour of an Al-Mg-Si industrial alloy, Mat. Science Engng. A 302 (2001), 300-307.

[3] Asserin-Lebert, A., Bron, F., Besson, J., and Gourgues, A.F.: Rupture of 6056 aluminium sheet materials: Effect of sheet thickness on strain localisation and toughness, Proc. 14th Bienniel Conf. on Fracture (ECF 14), EMAS Publ., 2002, 97-104.

[4] Hval, M., Thaulow, C., Lange, J.H., Hoeydal, S.H., and Zhang, Z.L.: Numerical modlling of ductile fracture behavior in aluminium weldments, Welding Research Supplement (1998), 208-217.

[5] Gurson, A.L.: Continuum theory of ductile rupture by void nucleation and growth: Part I - Yield Criteria and Flow Rules for Porous Ductile Media, J. Engng. Materials and Technology 99 (1977), 2-15.

[6] Needleman, A. and Tvergaard, V.: An analysis of ductile rupture at a crack tip, J. Mech. Phys. Solids 35 (1987), 151-183.

[7] Ruggieri, C., Panontin, T.L., and Dodds, Numerical modelling of ductile crack growth in 3D using computational cell elements, Int. J. Fracture 82 (1996), 67-95.

[8] Siegmund, T., and Brocks, W.: Prediction of the work of separation and implications to modelling. Int. J. Fracture 99 (1999), 97-116.

[9] Nègre, P., Steglich, D., and Brocks, W.: Crack extension in aluminium welds: A numerical approach using the Gurson-Tvergaard-Needleman model, submitted for publication in Engineering Fracture Mechanics

[10] Scheider, I., and Brocks, W.: Simulation of cup-cone fracture in round bars using the cohesive zone model, Engineering Fracture Mechanics 70 (2003), 1943-1961.

[11] Cornec, A., Scheider, I., and Schwalbe, K.-H.: On the practical application of the cohesive model, Engineering Fracture Mechanics 70 (2003) 1963-1987.

[12] Schwalbe, K.-H., Heerens, J., Zerbst, U., Pisarski, H., and Koçak, M.: The GKSS test procedure for determining the fracture behaviour of materials: EFAM GTP 02, Technical Report GKSS 2002/24, Geesthacht, 2002.